BABAR-CONF-04/20
SLAC-PUB-10610
August 2004

Measurement of the Branching Fractions for the Decays $B^0 \to D^{*-} p\overline{p}\pi^+$, $B^0 \to D^- p\overline{p}\pi^+$, $B^0 \to \overline{D}^{*0} p\overline{p}$ and $B^0 \to \overline{D}^0 p\overline{p}$

The *BABAR* Collaboration

February 7, 2008

Abstract

The B^0 meson decay modes $B^0 \to D^{*-} p\overline{p}\pi^+, D^- p\overline{p}\pi^+, \overline{D}^{*0} p\overline{p}$, and $B^0 \to \overline{D}^0 p\overline{p}$ are studied in a sample of 124×10^6 $B\overline{B}$ pairs collected with the *BABAR* detector at the PEP-II collider. The decay of $B^0 \to D^- p\overline{p}\pi^+$ is observed for the first time, with a measured branching fraction $\mathcal{B}(B^0 \to D^- p\overline{p}\pi^+) = (3.80 \pm 0.35 \pm 0.46) \times 10^{-4}$. The following branching fractions are also determined: $\mathcal{B}(B^0 \to D^{*-} p\overline{p}\pi^+) = (5.61 \pm 0.59 \pm 0.73) \times 10^{-4}$, $\mathcal{B}(B^0 \to \overline{D}^{*0} p\overline{p}) = (0.67 \pm 0.21 \pm 0.09) \times 10^{-4}$, and $\mathcal{B}(B^0 \to \overline{D}^0 p\overline{p}) = (1.24 \pm 0.14 \pm 0.12) \times 10^{-4}$. In each decay mode the invariant mass spectra of the charmed mesons and the baryons are compared with a pure phase-space hypothesis in order to gain insight into the B meson decay dynamics. In particular, the Dalitz plots of $\overline{D}^{*0} p$ versus $\overline{D}^{*0}\overline{p}$ for $B^0 \to \overline{D}^{*0} p\overline{p}$ and of $\overline{D}^0 p$ versus $\overline{D}^0\overline{p}$ for $B^0 \to \overline{D}^0 p\overline{p}$ are presented. All results are preliminary.

Submitted to the 32nd International Conference on High-Energy Physics, ICHEP 04,
16 August—22 August 2004, Beijing, China

Stanford Linear Accelerator Center, Stanford University, Stanford, CA 94309

Work supported in part by Department of Energy contract DE-AC03-76SF00515.

The *BABAR* Collaboration,

B. Aubert, R. Barate, D. Boutigny, F. Couderc, J.-M. Gaillard, A. Hicheur, Y. Karyotakis, J. P. Lees, V. Tisserand, A. Zghiche

Laboratoire de Physique des Particules, F-74941 Annecy-le-Vieux, France

A. Palano, A. Pompili

Università di Bari, Dipartimento di Fisica and INFN, I-70126 Bari, Italy

J. C. Chen, N. D. Qi, G. Rong, P. Wang, Y. S. Zhu

Institute of High Energy Physics, Beijing 100039, China

G. Eigen, I. Ofte, B. Stugu

University of Bergen, Inst. of Physics, N-5007 Bergen, Norway

G. S. Abrams, A. W. Borgland, A. B. Breon, D. N. Brown, J. Button-Shafer, R. N. Cahn, E. Charles, C. T. Day, M. S. Gill, A. V. Gritsan, Y. Groysman, R. G. Jacobsen, R. W. Kadel, J. Kadyk, L. T. Kerth, Yu. G. Kolomensky, G. Kukartsev, G. Lynch, L. M. Mir, P. J. Oddone, T. J. Orimoto, M. Pripstein, N. A. Roe, M. T. Ronan, V. G. Shelkov, W. A. Wenzel

Lawrence Berkeley National Laboratory and University of California, Berkeley, CA 94720, USA

M. Barrett, K. E. Ford, T. J. Harrison, A. J. Hart, C. M. Hawkes, S. E. Morgan, A. T. Watson

University of Birmingham, Birmingham, B15 2TT, United Kingdom

M. Fritsch, K. Goetzen, T. Held, H. Koch, B. Lewandowski, M. Pelizaeus, M. Steinke

Ruhr Universität Bochum, Institut für Experimentalphysik 1, D-44780 Bochum, Germany

J. T. Boyd, N. Chevalier, W. N. Cottingham, M. P. Kelly, T. E. Latham, F. F. Wilson

University of Bristol, Bristol BS8 1TL, United Kingdom

T. Cuhadar-Donszelmann, C. Hearty, N. S. Knecht, T. S. Mattison, J. A. McKenna, D. Thiessen

University of British Columbia, Vancouver, BC, Canada V6T 1Z1

A. Khan, P. Kyberd, L. Teodorescu

Brunel University, Uxbridge, Middlesex UB8 3PH, United Kingdom

A. E. Blinov, V. E. Blinov, V. P. Druzhinin, V. B. Golubev, V. N. Ivanchenko, E. A. Kravchenko, A. P. Onuchin, S. I. Serednyakov, Yu. I. Skovpen, E. P. Solodov, A. N. Yushkov

Budker Institute of Nuclear Physics, Novosibirsk 630090, Russia

D. Best, M. Bruinsma, M. Chao, I. Eschrich, D. Kirkby, A. J. Lankford, M. Mandelkern, R. K. Mommsen, W. Roethel, D. P. Stoker

University of California at Irvine, Irvine, CA 92697, USA

C. Buchanan, B. L. Hartfiel

University of California at Los Angeles, Los Angeles, CA 90024, USA

S. D. Foulkes, J. W. Gary, B. C. Shen, K. Wang

University of California at Riverside, Riverside, CA 92521, USA

D. del Re, H. K. Hadavand, E. J. Hill, D. B. MacFarlane, H. P. Paar, Sh. Rahatlou, V. Sharma

University of California at San Diego, La Jolla, CA 92093, USA

J. W. Berryhill, C. Campagnari, B. Dahmes, O. Long, A. Lu, M. A. Mazur, J. D. Richman, W. Verkerke

University of California at Santa Barbara, Santa Barbara, CA 93106, USA

T. W. Beck, A. M. Eisner, C. A. Heusch, J. Kroseberg, W. S. Lockman, G. Nesom, T. Schalk, B. A. Schumm, A. Seiden, P. Spradlin, D. C. Williams, M. G. Wilson

University of California at Santa Cruz, Institute for Particle Physics, Santa Cruz, CA 95064, USA

J. Albert, E. Chen, G. P. Dubois-Felsmann, A. Dvoretskii, D. G. Hitlin, I. Narsky, T. Piatenko, F. C. Porter, A. Ryd, A. Samuel, S. Yang

California Institute of Technology, Pasadena, CA 91125, USA

S. Jayatilleke, G. Mancinelli, B. T. Meadows, M. D. Sokoloff

University of Cincinnati, Cincinnati, OH 45221, USA

T. Abe, F. Blanc, P. Bloom, S. Chen, W. T. Ford, U. Nauenberg, A. Olivas, P. Rankin, J. G. Smith, J. Zhang, L. Zhang

University of Colorado, Boulder, CO 80309, USA

A. Chen, J. L. Harton, A. Soffer, W. H. Toki, R. J. Wilson, Q. Zeng

Colorado State University, Fort Collins, CO 80523, USA

D. Altenburg, T. Brandt, J. Brose, M. Dickopp, E. Feltresi, A. Hauke, H. M. Lacker, R. Müller-Pfefferkorn, R. Nogowski, S. Otto, A. Petzold, J. Schubert, K. R. Schubert, R. Schwierz, B. Spaan, J. E. Sundermann

Technische Universität Dresden, Institut für Kern- und Teilchenphysik, D-01062 Dresden, Germany

D. Bernard, G. R. Bonneaud, F. Brochard, P. Grenier, S. Schrenk, Ch. Thiebaux, G. Vasileiadis, M. Verderi

Ecole Polytechnique, LLR, F-91128 Palaiseau, France

D. J. Bard, P. J. Clark, D. Lavin, F. Muheim, S. Playfer, Y. Xie

University of Edinburgh, Edinburgh EH9 3JZ, United Kingdom

M. Andreotti, V. Azzolini, D. Bettoni, C. Bozzi, R. Calabrese, G. Cibinetto, E. Luppi, M. Negrini, L. Piemontese, A. Sarti

Università di Ferrara, Dipartimento di Fisica and INFN, I-44100 Ferrara, Italy

E. Treadwell

Florida A&M University, Tallahassee, FL 32307, USA

F. Anulli, R. Baldini-Ferroli, A. Calcaterra, R. de Sangro, G. Finocchiaro, P. Patteri, I. M. Peruzzi, M. Piccolo, A. Zallo

Laboratori Nazionali di Frascati dell'INFN, I-00044 Frascati, Italy

A. Buzzo, R. Capra, R. Contri, G. Crosetti, M. Lo Vetere, M. Macri, M. R. Monge, S. Passaggio, C. Patrignani, E. Robutti, A. Santroni, S. Tosi

Università di Genova, Dipartimento di Fisica and INFN, I-16146 Genova, Italy

S. Bailey, G. Brandenburg, K. S. Chaisanguanthum, M. Morii, E. Won

Harvard University, Cambridge, MA 02138, USA

R. S. Dubitzky, U. Langenegger

Universität Heidelberg, Physikalisches Institut, Philosophenweg 12, D-69120 Heidelberg, Germany

W. Bhimji, D. A. Bowerman, P. D. Dauncey, U. Egede, J. R. Gaillard, G. W. Morton, J. A. Nash, M. B. Nikolich, G. P. Taylor

Imperial College London, London, SW7 2AZ, United Kingdom

M. J. Charles, G. J. Grenier, U. Mallik

University of Iowa, Iowa City, IA 52242, USA

J. Cochran, H. B. Crawley, J. Lamsa, W. T. Meyer, S. Prell, E. I. Rosenberg, A. E. Rubin, J. Yi

Iowa State University, Ames, IA 50011-3160, USA

M. Biasini, R. Covarelli, M. Pioppi

Università di Perugia, Dipartimento di Fisica and INFN, I-06100 Perugia, Italy

M. Davier, X. Giroux, G. Grosdidier, A. Höcker, S. Laplace, F. Le Diberder, V. Lepeltier, A. M. Lutz, T. C. Petersen, S. Plaszczynski, M. H. Schune, L. Tantot, G. Wormser

Laboratoire de l'Accélérateur Linéaire, F-91898 Orsay, France

C. H. Cheng, D. J. Lange, M. C. Simani, D. M. Wright

Lawrence Livermore National Laboratory, Livermore, CA 94550, USA

A. J. Bevan, C. A. Chavez, J. P. Coleman, I. J. Forster, J. R. Fry, E. Gabathuler, R. Gamet, D. E. Hutchcroft, R. J. Parry, D. J. Payne, R. J. Sloane, C. Touramanis

University of Liverpool, Liverpool L69 72E, United Kingdom

J. J. Back,[1] C. M. Cormack, P. F. Harrison,[1] F. Di Lodovico, G. B. Mohanty[1]

Queen Mary, University of London, E1 4NS, United Kingdom

C. L. Brown, G. Cowan, R. L. Flack, H. U. Flaecher, M. G. Green, P. S. Jackson, T. R. McMahon, S. Ricciardi, F. Salvatore, M. A. Winter

University of London, Royal Holloway and Bedford New College, Egham, Surrey TW20 0EX, United Kingdom

D. Brown, C. L. Davis

University of Louisville, Louisville, KY 40292, USA

J. Allison, N. R. Barlow, R. J. Barlow, P. A. Hart, M. C. Hodgkinson, G. D. Lafferty, A. J. Lyon, J. C. Williams

University of Manchester, Manchester M13 9PL, United Kingdom

A. Farbin, W. D. Hulsbergen, A. Jawahery, D. Kovalskyi, C. K. Lae, V. Lillard, D. A. Roberts

University of Maryland, College Park, MD 20742, USA

G. Blaylock, C. Dallapiccola, K. T. Flood, S. S. Hertzbach, R. Kofler, V. B. Koptchev, T. B. Moore, S. Saremi, H. Staengle, S. Willocq

University of Massachusetts, Amherst, MA 01003, USA

[1]Now at Department of Physics, University of Warwick, Coventry, United Kingdom

R. Cowan, G. Sciolla, S. J. Sekula, F. Taylor, R. K. Yamamoto

Massachusetts Institute of Technology, Laboratory for Nuclear Science, Cambridge, MA 02139, USA

D. J. J. Mangeol, P. M. Patel, S. H. Robertson

McGill University, Montréal, QC, Canada H3A 2T8

A. Lazzaro, V. Lombardo, F. Palombo

Università di Milano, Dipartimento di Fisica and INFN, I-20133 Milano, Italy

J. M. Bauer, L. Cremaldi, V. Eschenburg, R. Godang, R. Kroeger, J. Reidy, D. A. Sanders, D. J. Summers, H. W. Zhao

University of Mississippi, University, MS 38677, USA

S. Brunet, D. Côté, P. Taras

Université de Montréal, Laboratoire René J. A. Lévesque, Montréal, QC, Canada H3C 3J7

H. Nicholson

Mount Holyoke College, South Hadley, MA 01075, USA

N. Cavallo,[2] F. Fabozzi,[2] C. Gatto, L. Lista, D. Monorchio, P. Paolucci, D. Piccolo, C. Sciacca

Università di Napoli Federico II, Dipartimento di Scienze Fisiche and INFN, I-80126, Napoli, Italy

M. Baak, H. Bulten, G. Raven, H. L. Snoek, L. Wilden

NIKHEF, National Institute for Nuclear Physics and High Energy Physics, NL-1009 DB Amsterdam, The Netherlands

C. P. Jessop, J. M. LoSecco

University of Notre Dame, Notre Dame, IN 46556, USA

T. Allmendinger, K. K. Gan, K. Honscheid, D. Hufnagel, H. Kagan, R. Kass, T. Pulliam, A. M. Rahimi, R. Ter-Antonyan, Q. K. Wong

Ohio State University, Columbus, OH 43210, USA

J. Brau, R. Frey, O. Igonkina, C. T. Potter, N. B. Sinev, D. Strom, E. Torrence

University of Oregon, Eugene, OR 97403, USA

F. Colecchia, A. Dorigo, F. Galeazzi, M. Margoni, M. Morandin, M. Posocco, M. Rotondo, F. Simonetto, R. Stroili, G. Tiozzo, C. Voci

Università di Padova, Dipartimento di Fisica and INFN, I-35131 Padova, Italy

M. Benayoun, H. Briand, J. Chauveau, P. David, Ch. de la Vaissière, L. Del Buono, O. Hamon, M. J. J. John, Ph. Leruste, J. Malcles, J. Ocariz, M. Pivk, L. Roos, S. T'Jampens, G. Therin

Universités Paris VI et VII, Laboratoire de Physique Nucléaire et de Hautes Energies, F-75252 Paris, France

P. F. Manfredi, V. Re

Università di Pavia, Dipartimento di Elettronica and INFN, I-27100 Pavia, Italy

[2]Also with Università della Basilicata, Potenza, Italy

P. K. Behera, L. Gladney, Q. H. Guo, J. Panetta

University of Pennsylvania, Philadelphia, PA 19104, USA

C. Angelini, G. Batignani, S. Bettarini, M. Bondioli, F. Bucci, G. Calderini, M. Carpinelli, F. Forti, M. A. Giorgi, A. Lusiani, G. Marchiori, F. Martinez-Vidal,[3] M. Morganti, N. Neri, E. Paoloni, M. Rama, G. Rizzo, F. Sandrelli, J. Walsh

Università di Pisa, Dipartimento di Fisica, Scuola Normale Superiore and INFN, I-56127 Pisa, Italy

M. Haire, D. Judd, K. Paick, D. E. Wagoner

Prairie View A&M University, Prairie View, TX 77446, USA

N. Danielson, P. Elmer, Y. P. Lau, C. Lu, V. Miftakov, J. Olsen, A. J. S. Smith, A. V. Telnov

Princeton University, Princeton, NJ 08544, USA

F. Bellini, G. Cavoto,[4] R. Faccini, F. Ferrarotto, F. Ferroni, M. Gaspero, L. Li Gioi, M. A. Mazzoni, S. Morganti, M. Pierini, G. Piredda, F. Safai Tehrani, C. Voena

Università di Roma La Sapienza, Dipartimento di Fisica and INFN, I-00185 Roma, Italy

S. Christ, G. Wagner, R. Waldi

Universität Rostock, D-18051 Rostock, Germany

T. Adye, N. De Groot, B. Franek, N. I. Geddes, G. P. Gopal, E. O. Olaiya

Rutherford Appleton Laboratory, Chilton, Didcot, Oxon, OX11 0QX, United Kingdom

R. Aleksan, S. Emery, A. Gaidot, S. F. Ganzhur, P.-F. Giraud, G. Hamel de Monchenault, W. Kozanecki, M. Legendre, G. W. London, B. Mayer, G. Schott, G. Vasseur, Ch. Yèche, M. Zito

DSM/Dapnia, CEA/Saclay, F-91191 Gif-sur-Yvette, France

M. V. Purohit, A. W. Weidemann, J. R. Wilson, F. X. Yumiceva

University of South Carolina, Columbia, SC 29208, USA

D. Aston, R. Bartoldus, N. Berger, A. M. Boyarski, O. L. Buchmueller, R. Claus, M. R. Convery, M. Cristinziani, G. De Nardo, D. Dong, J. Dorfan, D. Dujmic, W. Dunwoodie, E. E. Elsen, S. Fan, R. C. Field, T. Glanzman, S. J. Gowdy, T. Hadig, V. Halyo, C. Hast, T. Hryn'ova, W. R. Innes, M. H. Kelsey, P. Kim, M. L. Kocian, D. W. G. S. Leith, J. Libby, S. Luitz, V. Luth, H. L. Lynch, H. Marsiske, R. Messner, D. R. Muller, C. P. O'Grady, V. E. Ozcan, A. Perazzo, M. Perl, S. Petrak, B. N. Ratcliff, A. Roodman, A. A. Salnikov, R. H. Schindler, J. Schwiening, G. Simi, A. Snyder, A. Soha, J. Stelzer, D. Su, M. K. Sullivan, J. Va'vra, S. R. Wagner, M. Weaver, A. J. R. Weinstein, W. J. Wisniewski, M. Wittgen, D. H. Wright, A. K. Yarritu, C. C. Young

Stanford Linear Accelerator Center, Stanford, CA 94309, USA

P. R. Burchat, A. J. Edwards, T. I. Meyer, B. A. Petersen, C. Roat

Stanford University, Stanford, CA 94305-4060, USA

S. Ahmed, M. S. Alam, J. A. Ernst, M. A. Saeed, M. Saleem, F. R. Wappler

State University of New York, Albany, NY 12222, USA

[3]Also with IFIC, Instituto de Física Corpuscular, CSIC-Universidad de Valencia, Valencia, Spain
[4]Also with Princeton University, Princeton, USA

W. Bugg, M. Krishnamurthy, S. M. Spanier
University of Tennessee, Knoxville, TN 37996, USA

R. Eckmann, H. Kim, J. L. Ritchie, A. Satpathy, R. F. Schwitters
University of Texas at Austin, Austin, TX 78712, USA

J. M. Izen, I. Kitayama, X. C. Lou, S. Ye
University of Texas at Dallas, Richardson, TX 75083, USA

F. Bianchi, M. Bona, F. Gallo, D. Gamba
Università di Torino, Dipartimento di Fisica Sperimentale and INFN, I-10125 Torino, Italy

L. Bosisio, C. Cartaro, F. Cossutti, G. Della Ricca, S. Dittongo, S. Grancagnolo, L. Lanceri, P. Poropat,[5] L. Vitale, G. Vuagnin
Università di Trieste, Dipartimento di Fisica and INFN, I-34127 Trieste, Italy

R. S. Panvini
Vanderbilt University, Nashville, TN 37235, USA

Sw. Banerjee, C. M. Brown, D. Fortin, P. D. Jackson, R. Kowalewski, J. M. Roney, R. J. Sobie
University of Victoria, Victoria, BC, Canada V8W 3P6

H. R. Band, B. Cheng, S. Dasu, M. Datta, A. M. Eichenbaum, M. Graham, J. J. Hollar, J. R. Johnson, P. E. Kutter, H. Li, R. Liu, A. Mihalyi, A. K. Mohapatra, Y. Pan, R. Prepost, P. Tan, J. H. von Wimmersperg-Toeller, J. Wu, S. L. Wu, Z. Yu
University of Wisconsin, Madison, WI 53706, USA

M. G. Greene, H. Neal
Yale University, New Haven, CT 06511, USA

[5]Deceased

1 INTRODUCTION

The very successful performance of the two B factories PEP II and KEKB enables the study of B meson decays with unprecedented sensitivity. In this paper B meson decays to final states which include a charmed meson and a baryon anti-baryon pair are studied. The observation of the $B^0 \to D^{*-}p\overline{p}\pi^+$ and $B^0 \to D^{*-}p\overline{n}$ decays by CLEO [1], and the color-suppressed $B^0 \to \overline{D}^0 p\overline{p}$ and $B^0 \to \overline{D}^{*0} p\overline{p}$ decay modes by Belle [2] suggest the dominance of multi-body final states in decays of B mesons into baryons [3]. In this paper we present the measurements of the branching fractions for the following four decay modes: $B^0 \to D^{*-}p\overline{p}\pi^+$, $B^0 \to D^{-}p\overline{p}\pi^+$, $B^0 \to \overline{D}^{*0} p\overline{p}$, and $B^0 \to \overline{D}^{0} p\overline{p}$. Observation of modes proposed here would help clarify the dynamics of weak decays of B involving baryons [4].

Since the branching fractions of multi-body decays are sizable [5], it is natural to ask whether such final states are actually the products of an intermediate two-body channel. If this is the case, then these initial two-body decays may involve a baryon-antibaryon bound states ($N\overline{N}$) [6, 7] or a charmed pentaquark (DN, which can be $\overline{c}uudd$ for example) [8, 9] or a (nonexotic) heavy charmed baryon. Motivated by these considerations, the invariant mass spectrum of the baryon-antibaryon and the invariant mass spectra of the charmed meson and baryon are investigated. In particular, the Dalitz plots for $\overline{D}^{*0}p$ versus $\overline{D}^{*0}\overline{p}$ and $\overline{D}^{0}p$ versus $\overline{D}^{0}\overline{p}$ for the $B^0 \to \overline{D}^{0} p\overline{p}$ and $B^0 \to \overline{D}^{*0} p\overline{p}$ decay modes, respectively, are presented. The inclusion of the charge conjugate modes is implicit throughout this report.

2 THE *BABAR* DETECTOR AND DATASET

The data used in this analysis were collected with the *BABAR* detector at the PEP-II storage ring. The sample corresponds to an integrated luminosity of $112.5\,\mathrm{fb}^{-1}$ at the $\Upsilon(4S)$ resonance (on-resonance) and $11.9\,\mathrm{fb}^{-1}$ taken 40 MeV below the $\Upsilon(4S)$ resonance (off-resonance). The on-resonance sample contains about 124.1×10^6 $B\overline{B}$ pairs. The collider is operated with asymmetric beam energies, producing a boost of $\beta\gamma \approx 0.56$ of the $\Upsilon(4S)$ along the collision axis.

The *BABAR* detector is optimized for asymmetric energy collisions at a center-of-mass (CM) energy corresponding to the $\Upsilon(4S)$ resonance. The detector is described in detail in reference [10]. Charged particle tracking is provided by a five-layer double-sided silicon vertex tracker (SVT) and a 40-layer drift chamber (DCH) contained within the magnetic field of a 1.5T superconducting solenoid. The tracking system provides momentum reconstruction of charged particles and measures energy-loss (dE/dx) for particle identification. Additional charged K–π particle identification is provided by a ring-imaging Cherenkov detector (DIRC), which exploits the total internal reflection of Cherenkov photons within synthetic quartz bars. The energies of neutral particles are measured by an electromagnetic calorimeter (EMC) composed of 6580 CsI(Tl) crystals. The magnetic flux return of the solenoid (IFR) is instrumented with resistive plate chambers in order to provide muon and neutral hadron identification.

A GEANT4-based [11] Monte Carlo (MC) simulation is used to model the signal efficiency and the physics backgrounds. Simulation samples equivalent to approximately three times the accumulated data were used to model $B\overline{B}$ events, and samples equivalent to approximately one times the accumulated data were used to model $e^+e^- \to u\overline{u}$, $d\overline{d}$, $s\overline{s}$, and $c\overline{c}$ events.

3 ANALYSIS METHOD

The B^0 meson is reconstructed in the following four decay modes: $B^0 \to D^{*-}p\overline{p}\pi^+$, $B^0 \to D^-p\overline{p}\pi^+$, $B^0 \to \overline{D}^{*0}p\overline{p}$, and $B^0 \to \overline{D}^0p\overline{p}$. The D^{*-} and $\overline{D}^{*0}$ are reconstructed as $\overline{D}^0\pi^-$ and $\overline{D}^0\pi^0$, respectively. The D^- candidates are reconstructed in the decay mode $K^+\pi^-\pi^-$. The $\overline{D}^0$ candidates are reconstructed in the $K^+\pi^-$ mode.

3.1 B^0 SELECTION

The B^0 reconstruction proceeds as follows. First we reconstruct the D^- and $\overline{D}^0$ candidates in the decay modes noted above. For all decay modes, charged kaons are distinguished from the pions and protons with energy-loss (dE/dx) information in the tracking system and the Cherenkov angle and the number of photons measured by the DIRC. For the $B^0 \to \overline{D}^{*0}p\overline{p}$ decay mode only, the pion from $\overline{D}^0 \to K^+\pi^-$ decay must not be identified as either an electron, muon, kaon or proton. The mass of the reconstructed $\overline{D}^0$ or D^- candidates must be within 3 standard deviations of the fitted mean of reconstructed $\overline{D}^0$ or D^- mass for each decay mode. Finally, the daughter tracks from the $\overline{D}^0$ or D^- are required to be consistent with originating from a common vertex.

For the decay modes $B^0 \to D^{*-}p\overline{p}\pi^+$ and $B^0 \to \overline{D}^{*0}p\overline{p}$, D^{*-} and $\overline{D}^{*0}$ candidates are reconstructed by combining the $\overline{D}^0$ candidate with a soft track or a soft π^0, respectively. The momentum of the soft track or soft π^0 in the CM frame must be less than 0.45 GeV/c. The π^0 candidate is required to have a two-photon invariant mass between 0.116–0.150 GeV/c^2, and its daughter photon candidates must have a minimum cluster energy of 30 MeV. The mass difference between D^* and D^0 ($\Delta M = m_{D^*} - m_{D^0}$) is required to be less than 0.1486 GeV/c^2 and 0.1453 GeV/c^2 for D^{*-} and $\overline{D}^{*0}$ candidates, respectively. The ΔM requirement removes crossfeed from $B^0 \to \overline{D}^{*0}p\overline{p}$ into $B^0 \to \overline{D}^0p\overline{p}$. For each track except for the soft pion from D^{*-} decays, the transverse momentum p_T must be larger than 0.1 GeV/c in order to improve the quality of the vertex fit.

To reconstruct the candidate $B^0 \to D^{*-}p\overline{p}\pi^+$ and $B^0 \to D^-p\overline{p}\pi^+$ decay modes, both proton and anti-proton candidates are distinguished from pions and kaons on the basis of energy-loss (dE/dx) information in the tracking system and the Cherenkov angle and the number of photons measured by DIRC. The reconstructed D^{*-} and D^-, respectively, are combined with an identified proton and anti-proton pair and a track. We require that the pion candidate track must not be identified as either an electron, a muon, a kaon or a proton. For the decay modes $B^0 \to \overline{D}^{*0}p\overline{p}$ and $B^0 \to \overline{D}^0p\overline{p}$, the $\overline{D}^{*0}$ and $\overline{D}^0$ candidates, respectively, are combined with an identified proton and anti-proton pair. All the daughters of the B^0 must originate from a common vertex.

Two additional kinematic variables are used to identify the reconstructed B^0 candidates [10]. The first is the beam-energy-substituted mass, $m_{ES} = [(E^2_{CM}/2 + \mathbf{p}_i \cdot \mathbf{p}_B)^2/E_i^2 - \mathbf{p}_B^2]^{1/2}$, where E_{CM} is the total CM energy of the e^+e^- collision, $(E_i, \mathbf{p}_i)$ is the four-momentum of the initial e^+e^- system and $\mathbf{p}_B$ is the momentum of the reconstructed B candidate, both measured in the laboratory frame. The second variable is $\Delta E = E^*_B - E_{CM}/2$, where E^*_B is the B-candidate energy in the CM frame. The B meson candidates are defined by requiring: $5.20\,\mathrm{GeV}/c^2 < m_{\mathrm{ES}} < 5.29$ GeV/c^2 and $|\Delta E| < 0.12$ GeV. These two variables are then used in a maximum likelihood fit to extract signal and background yields.

If more than one suitable B^0 candidate is reconstructed in an event, then for each B^0 decay mode one best candidate is selected. The best candidate selection algorithm is based on a χ^2-like quantity constructed from the difference between the D mass and/or mass difference ΔM for the candidate and the nominal value [12]. For a given event, the candidate with the lowest value of χ^2

is selected for each B^0 decay mode. For the $B^0 \to D^{*-}p\overline{p}\pi^+$ and $B^0 \to \overline{D}^{*0}p\overline{p}$ decays, the best candidate is selected based on the mass of the $\overline{D}^0$ candidate and ΔM. For the $B^0 \to D^-p\overline{p}\pi^+$ and $B^0 \to \overline{D}^0p\overline{p}$ decay modes, the reconstructed D meson mass is used for best candidate selection.

To suppress background from two-jet-like $e^+e^- \to q\bar{q}$ continuum, variables that characterize the event topology are used. We require $\cos\theta_{thr} < 0.9$, where θ_{thr} is the angle between the thrust axis of the B^0 candidate and that of the rest of the event. This requirement eliminates 63% of the continuum background and retains 88% of the signal events. For further continuum background suppression we require that the ratio of the second to zeroth Fox-Wolfram moments [13] is less than 0.35.

The signal efficiency in each B decay mode after applying all selection criteria is shown in Table 1. The efficiencies listed in the table are obtained from signal MC simulation assuming pure phase-space for the B decay model.

Table 1: Summary of selection efficiencies obtained from MC simulation based on a phase-space model and fitted yields from data for the B decay modes in this report. The error on the efficiency comes from the Monte Carlo statistics. The statistical significance is calculated as $\sqrt{2\Delta\log\mathcal{L}}$, where $\Delta\log\mathcal{L}$ is the log-likelihood difference between a signal hypothesis corresponding to the yield and that corresponding to a null yield.

Mode	Efficiency, %	Signal yield	Statistical significance
$B^0 \to D^{*-}p\overline{p}\pi^+$	6.97 ± 0.10	130±14	18σ
$B^0 \to D^-p\overline{p}\pi^+$	5.87 ± 0.10	238±22	17σ
$B^0 \to \overline{D}^{*0}p\overline{p}$	5.53 ± 0.09	13± 4	5σ
$B^0 \to \overline{D}^0p\overline{p}$	16.53± 0.15	96 ± 11	17σ

3.2 THE MAXIMUM LIKELIHOOD FIT

We perform an unbinned extended maximum likelihood (ML) fit to extract the signal and background yields. The variables $m_{\rm ES}$, ΔE are used to separate signal from backgrounds. The data sample is assumed to consist of signal and combinatorial backgrounds, which arise from random combinations of charged or neutral candidates from both continuum and $B\overline{B}$ events. The extended likelihood for a sample of N candidates is

$$\mathcal{L} = e^{-N'} \cdot \prod_{i=1}^{N} \{N_{sig} \cdot \mathcal{P}_{sig}(m_{ESi}, \Delta E_i) + N_{bkg} \cdot \mathcal{P}_{bkg}(m_{ESi}, \Delta E_i)\} \quad (1)$$

where N_{sig} and N_{bkg} are the number of signal and background yields (to be determined by the fit), respectively, and $N' = N_{sig}+N_{bkg}$. The probability density functions (PDFs) $\mathcal{P}_{sig}$ and $\mathcal{P}_{bkg}$ are the product of the PDFs of two discriminating variables. The signal PDF is thus given by $\mathcal{P}_{sig} = \mathcal{P}(m_{ESi}) \cdot \mathcal{P}(\Delta E_i)$. The signal PDFs are decomposed into two parts with distinct distributions:

- Signal class I: signal events that are correctly reconstructed or signal events that are misreconstructed due to a random slow π^- or π^0 assigned to a D^{*-} or D^{*0} decay. Since the $m_{\rm ES}$ and ΔE distributions for these two kinds of events do not significantly differ from each other, we put them into one signal class in the ML fit.

- Signal class II: signal events that are misreconstructed due to wrong tracks from B direct decays or from a wrongly reconstructed D meson. The $m_{\rm ES}$ and ΔE distributions are significantly different from those of signal class I. Hereafter signal class II events are also called Self-Cross-Feed (SCF) events. The fraction of this kind of misreconstructed signal event is estimated by MC simulation.

The PDFs of $m_{\rm ES}$ and ΔE for signal events are taken from the MC simulation, with the exception that the means of the signal Gaussian for the $m_{\rm ES}$ and ΔE PDFs are free to vary in the fit. The m_{ES} and ΔE PDFs for the combinatorial backgrounds, which include B background and continuum background, are described by two free parameters. One of these is from an ARGUS function [14] used to describe the $m_{\rm ES}$ shape, the other is from a first-order polynomial for the ΔE shape. A total of six parameters, including signal and background yields and all the parameters related to background PDFs, are varied in the fit.

4 PHYSICS RESULTS

The signal yield from the ML fit and statistical significance for each of the B modes are summarized in Table 1. The statistical significance is calculated as $\sqrt{2\Delta \log \mathcal{L}}$, where $\Delta \log \mathcal{L}$ is the log-likelihood difference between a signal hypothesis corresponding to the yield and that corresponding to a null yield. Figure 1 shows projection plots of $m_{\rm ES}$ and ΔE from the likelihood fit. The fit shows satisfactory agreement with distributions of the discriminating variables.

To correct for the efficiency variation across the Dalitz plot, which is of order 20% for $B^0 \to \overline{D}^{*0} p\overline{p}$ and 5% for $B^0 \to \overline{D}^0 p\overline{p}$ three-body decays, each event is assigned a signal weight, W_{sig}, which takes correlations into account:

$$W_{sig} = \frac{\sum_j V_{sig,j} \mathcal{P}(m_{\rm ES}, \Delta E)}{\sum_j N_j \mathcal{P}(m_{\rm ES}, \Delta E)} \tag{2}$$

where N_j is the number of events, $\mathcal{P}(m_{\rm ES}, \Delta E)$ is the PDF of the j^{th} component given the event values of $m_{\rm ES}$ and ΔE, and $V_{sig,j}$ is the signal row of the covariance matrix of the components yields obtained from the likelihood fit. We determine the efficiency as a function of position on the Dalitz plot from simulated signal events. The branching fractions of $B^0 \to \overline{D}^{*0} p\overline{p}$ and $B^0 \to \overline{D}^0 p\overline{p}$ three-body decays are corrected by the Dalitz plot dependent efficiencies. The effect of the D^{*-} polarization in the $B^0 \to \overline{D}^{*0} p\overline{p}$ mode is neglected in this Dalitz plot dependent efficiency correction.

We estimate the efficiencies for 4-body decays with the same method as for three-body decays. We find that the differences are 7.5% and 3.1% from the efficiencies obtained from a pure phase-space MC for the $B^0 \to D^{*-} p\overline{p}\pi^+$ and $B^0 \to D^- p\overline{p}\pi^+$, respectively. We will assign 7.5% and 3.1% as additional systematic errors for the two four-body decays, respectively.

In each of the four B decay modes, the signal region is defined as: $-0.035 < \Delta E < 0.03$ GeV and $m_{\rm ES} > 5.27$ GeV. The $m_{\rm ES}$ distributions after applying the requirement $-0.035 < \Delta E < 0.03$ GeV, and ΔE distributions after applying the requirement $m_{\rm ES} > 5.27$ GeV/c^2, are shown in Fig. 2 for all four decay modes. We also compare the invariant mass spectra for charmed meson and baryon combinations with a pure phase space hypothesis for B decays. Figure 3 shows the invariant mass of $D^{*-}p$ and $D^{*-}\overline{p}$ for signal candidates in the $B^0 \to D^{*-} p\overline{p}\pi^+$ mode. The open histogram is the expected distribution from $B^0 \to D^{*-} p\overline{p}\pi^+$ phase space signal MC simulation which is normalized to the fitted signal yield in data. The cross-hatched histograms describe the contributions from different background processes, which is normalized to the fitted background yield in data.

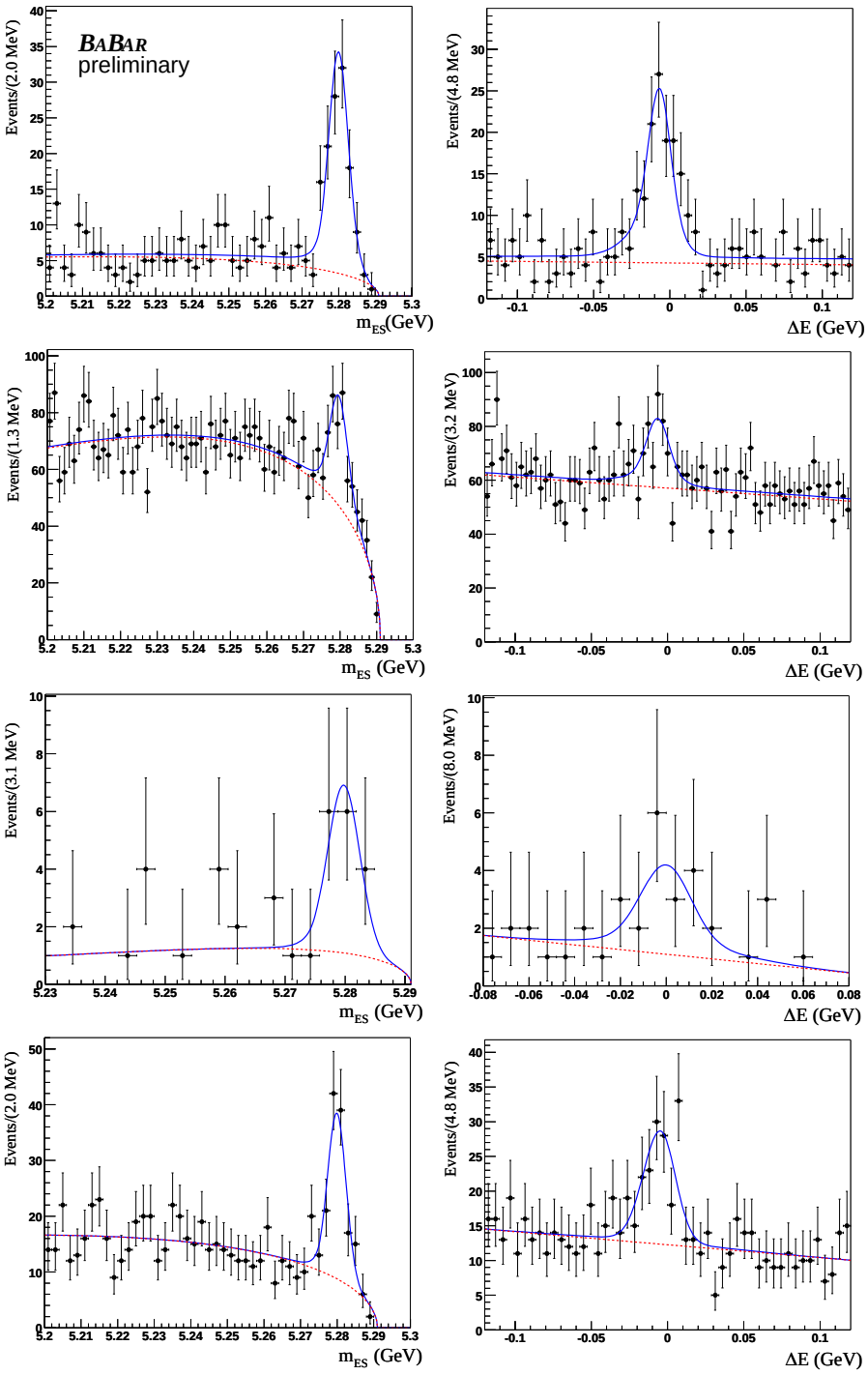

Figure 1: $m_{\rm ES}$ (left-hand column) and ΔE (right-hand column) distributions in data. The plots from top to bottom are for $B^0 \to D^{*-}p\overline{p}\pi^+$, $B^0 \to D^{-}p\overline{p}\pi^+$, $B^0 \to \overline{D}^{*0}p\overline{p}$, and $B^0 \to \overline{D}^{0}p\overline{p}$, respectively. The solid curve represents a projection of the maximum likelihood fit. The dashed curve represents the contribution from combinatorial background.

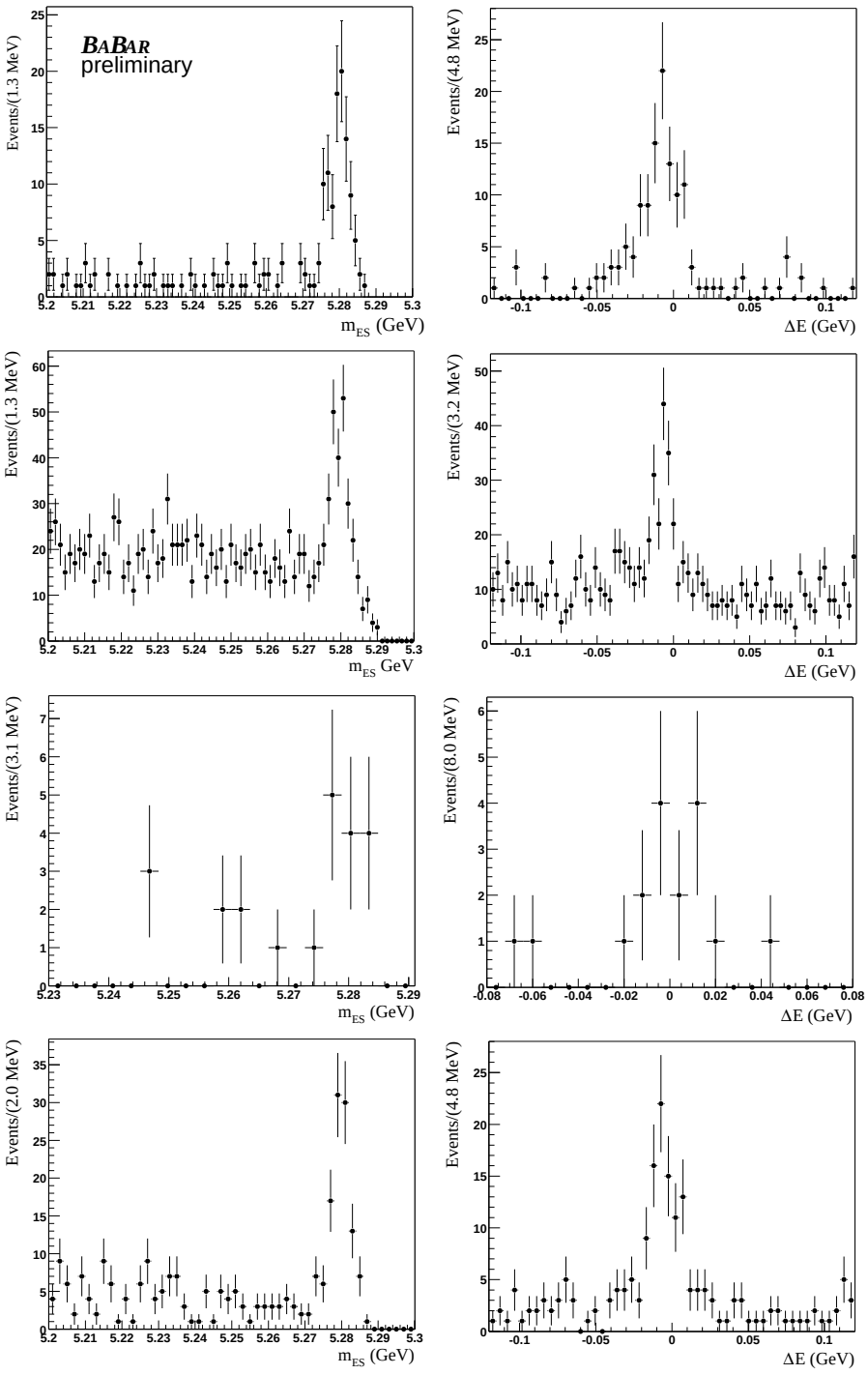

Figure 2: $m_{\rm ES}$ (left-hand column) distributions from data after applying requirement $-0.035 < \Delta E < 0.03$ GeV. The ΔE (right-hand column) distributions from data after applying requirement $m_{\rm ES} > 5.27$ GeV/c^2. The plots from top to bottom are for $B^0 \to D^{*-}p\overline{p}\pi^+$, $B^0 \to D^-p\overline{p}\pi^+$, $B^0 \to \overline{D}^{*0}p\overline{p}$, and $B^0 \to \overline{D}^0p\overline{p}$, respectively.

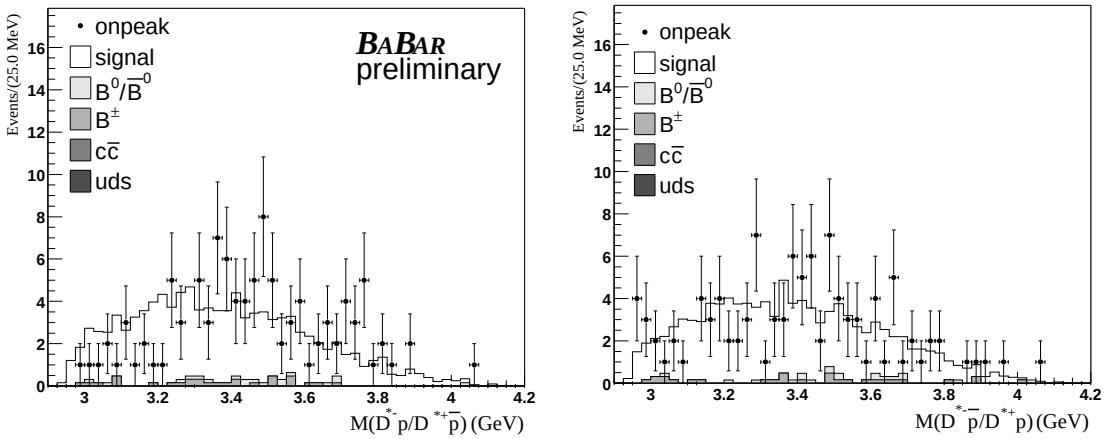

Figure 3: The invariant mass distribution of $D^{*-}p$ (left) and $D^{*-}\overline{p}$ (right) combinations from signal candidates in the $B^0 \to D^{*-}p\overline{p}\pi^+$ decay mode. The cross-hatched histograms describe the contributions from different background processes. The open histogram is the expected contribution from $B^0 \to D^{*-}p\overline{p}\pi^+$ phase space signal MC simulation.

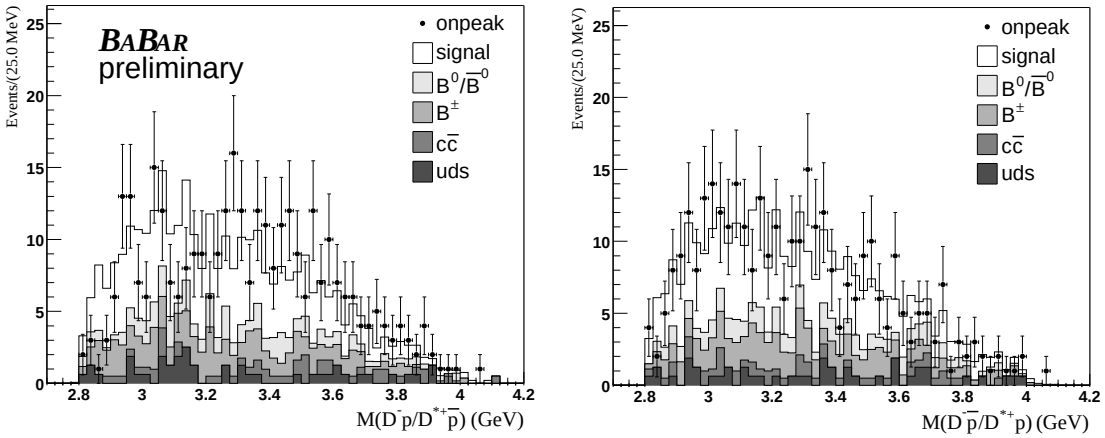

Figure 4: The invariant mass distribution of $D^{-}p$ (left) and $D^{-}\overline{p}$ (right) combinations from signal candidates in the $B^0 \to D^{-}p\overline{p}\pi^+$ decay mode. The cross-hatched histograms describe the contributions from different background processes. The open histogram is the expected contribution from the $B^0 \to D^{-}p\overline{p}\pi^+$ phase space signal MC simulation.

The shape of the invariant mass spectra in Fig. 3 show that the $D^{*-}p$ distribution in data is only marginally consistent with a phase space model, while the $D^{*-}\overline{p}$ is quite consistent with phase space. A similar observation holds for the $D^{-}p$ and $D^{-}\overline{p}$ distribution from signal candidates in the mode $B^0 \to D^{-}p\overline{p}\pi^+$ as shown in Fig. 4.

As shown in Fig. 5, the shapes of the invariant mass spectra from a phase-space model for the $\overline{D}^{*0}p$ and $\overline{D}^{*0}\overline{p}$ distributions in the $B^0 \to \overline{D}^{*0}p\overline{p}$ mode, are consistent with data given the current low statistics. However, the shape for the $\overline{D}^{0}p$ distribution in the $B^0 \to \overline{D}^{0}p\overline{p}$ mode is inconsistent and it appears to deviate from the phase-space expectation, as illustrated in the left-hand plot

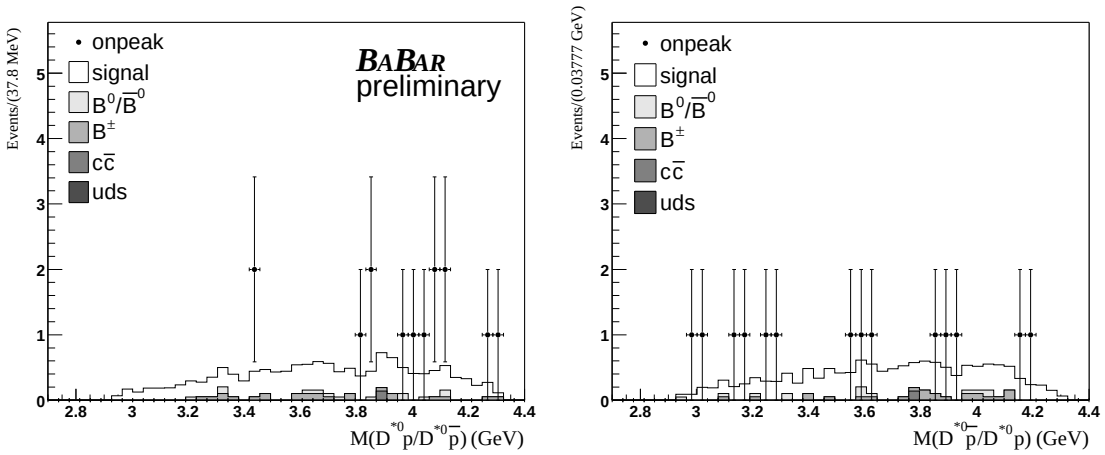

Figure 5: The invariant mass distribution of $\overline{D}^{*0}p$ (left) and $\overline{D}^{*0}\overline{p}$ (right) combinations from signal candidates in the $B^0 \to \overline{D}^{*0}p\overline{p}$ decay mode. The cross-hatched histograms describe the contributions from different background processes. The open histogram is the expected contribution from the $B^0 \to \overline{D}^{*0}p\overline{p}$ phase space signal MC simulation.

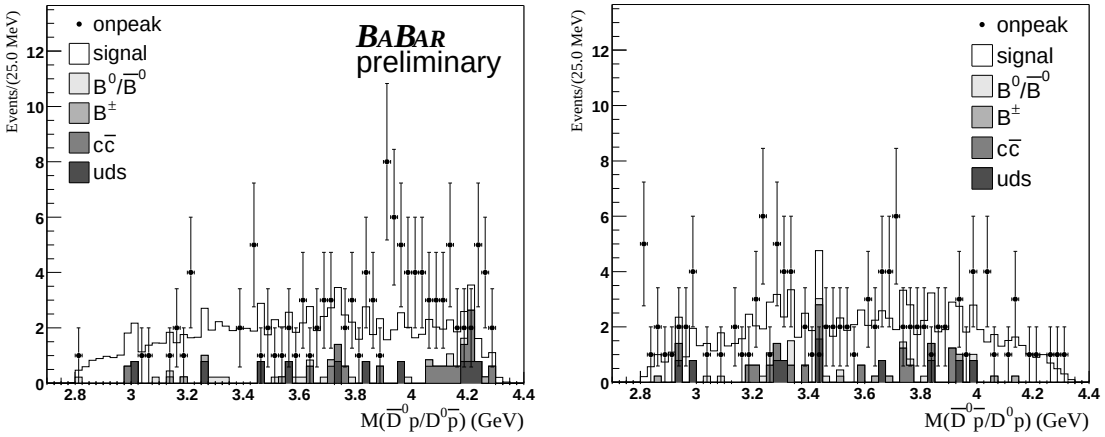

Figure 6: The invariant mass distribution of $\overline{D}^{0}p$ (left) and $\overline{D}^{0}\overline{p}$ (right) combinations from signal candidates in the $B^0 \to \overline{D}^{0}p\overline{p}$ decay mode. The cross-hatched histograms describe the contributions from different background processes. The open histogram is the expected contribution from the $B^0 \to \overline{D}^{0}p\overline{p}$ phase space signal MC simulation.

of Fig. 6. For $\overline{D}^{0}\overline{p}$, the distribution in data is consistent with the phase space, as shown in the right-hand plot of Fig. 6.

To further compare the observed mass distributions in data with uniform phase space, we show the Dalitz plot distributions for the two three-body decay modes in Figures 7 and 8. The distribution of $m^2(\overline{D}^{*0}p)$ versus $m^2(\overline{D}^{*0}\overline{p})$ for signal candidates in the $B^0 \to \overline{D}^{*0}p\overline{p}$ mode is shown in Figure 7; the distribution between $m^2(\overline{D}^{0}p)$ and $m^2(\overline{D}^{0}\overline{p})$ for the $B^0 \to \overline{D}^{0}p\overline{p}$ mode is shown in Figure 8. The triangles and dots correspond to data and the phase space MC simulation. Figure 7 shows a Dalitz plot for the mode $B^0 \to \overline{D}^{*0}p\overline{p}$. The comparison with the phase space distribution

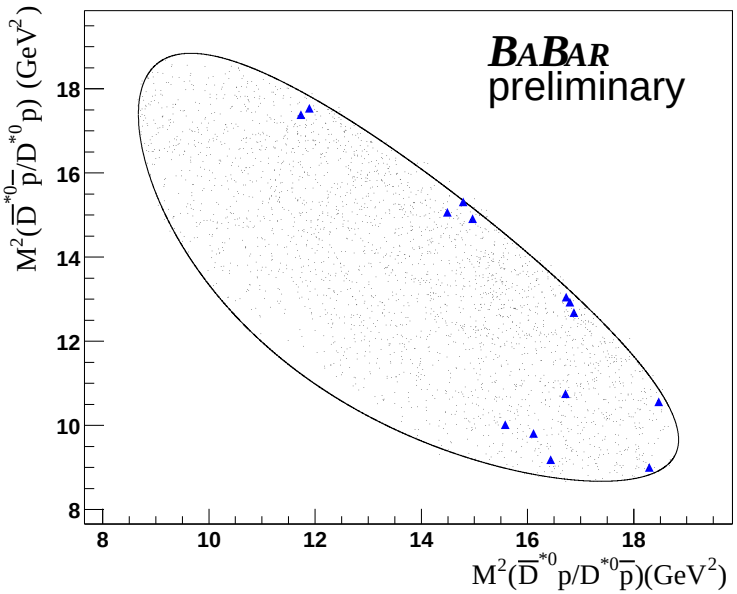

Figure 7: Dalitz plot for the mode $B^0 \to \overline{D}^{*0} p\overline{p}$. The horizontal and vertical axes correspond to the squared invariant masses of the $\overline{D}^{*0} p$ and $\overline{D}^{*0}\overline{p}$, respectively. The triangles and dots correspond to signal events in data and the phase space simulation, respectively.

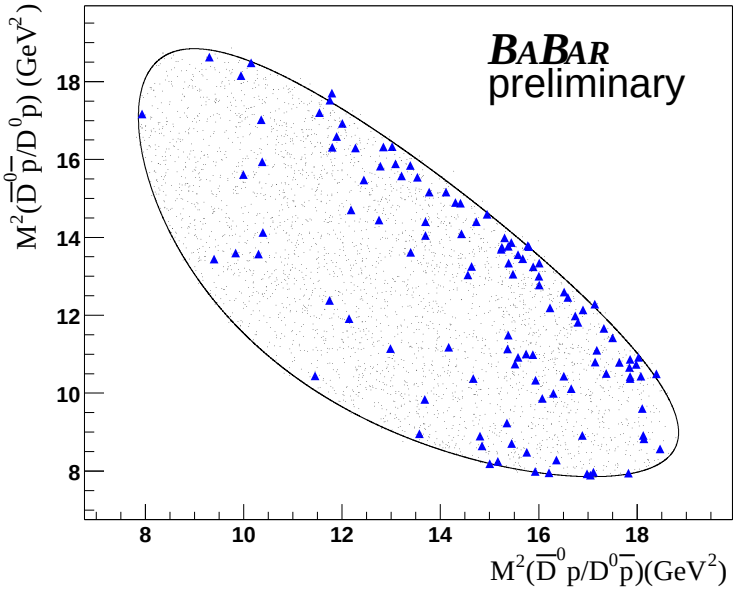

Figure 8: Dalitz plot for the mode $B^0 \to \overline{D}^0 p\overline{p}$. The horizontal and vertical axes correspond to the squared invariant masses of the $\overline{D}^0 p$ and $\overline{D}^0\overline{p}$, respectively. The triangles and dots correspond to signal events in data and the phase space simulation, respectively.

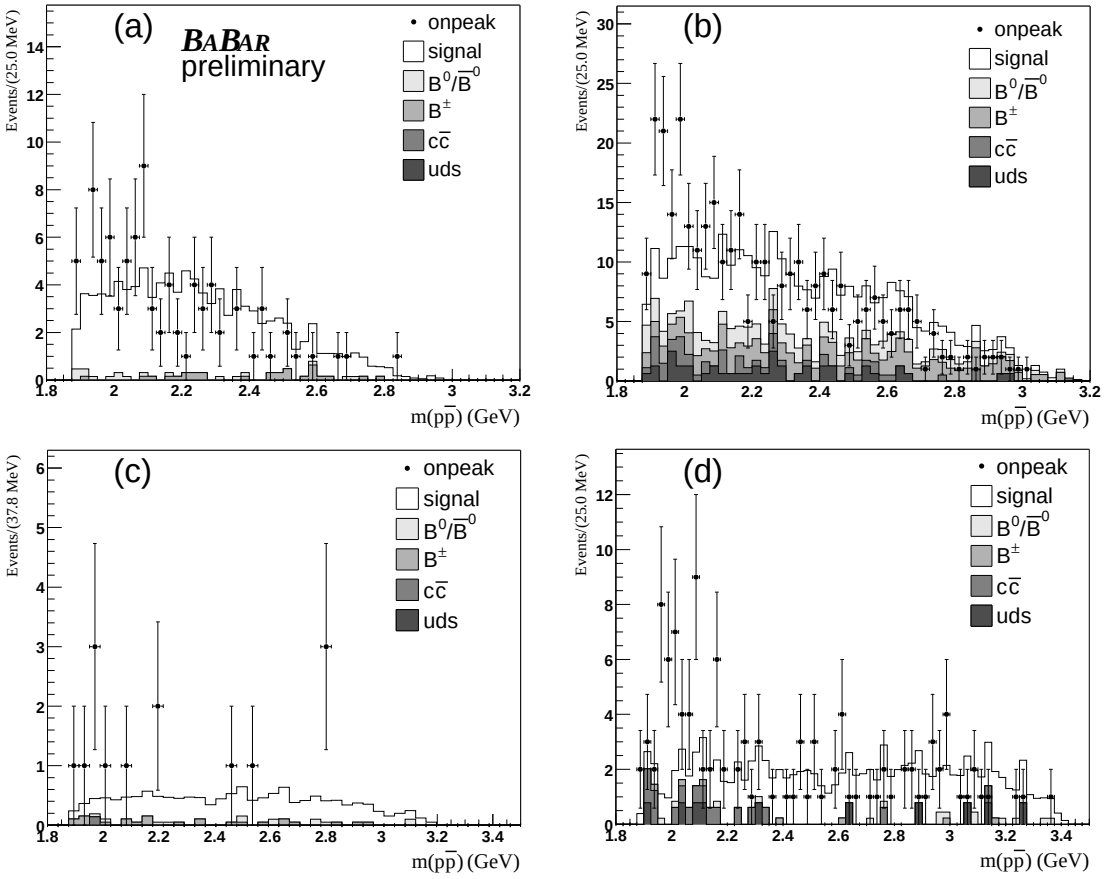

Figure 9: Invariant mass distributions for $p\overline{p}$ pairs in the signal sample for (a) for $B^0 \to D^{*-}p\overline{p}\pi^+$; (b) for $B^0 \to D^-p\overline{p}\pi^+$; (c) for $B^0 \to \overline{D}^{*0}p\overline{p}$; and (d) for $B^0 \to \overline{D}^0p\overline{p}$, respectively. The cross-hatched histograms describe the contributions from different background processes. The open histogram is the expected contribution from the phase space signal MC simulation.

is limited by low statistics. The equivalent plot for the mode $B^0 \to \overline{D}^0 p\overline{p}$, shown in Figure 8, shows a deviation from the pure phase space model. In addition, the Dalitz plots display a threshold enhancement in the $p\overline{p}$ invariant mass spectrum. Figure 9 shows the invariant masses of $p\overline{p}$ for each B decay mode. A threshold enhancement is observed for each B decay mode. A similar effect has also been observed by other experiments [2, 16].

The compatibility of data and MC simulation was quantified by means of a Kolmogorov-Smirnov test. Table 2 shows the probabilities of compatibility of data and MC simulation, where the shape of the data points and the MC histograms shown in Figures 3-6 and 9 were compared. The first and second columns correspond to the invariant mass spectra of the relevant D-meson and p combination (the corresponding minimal quark content is given in parentheses). Charge conjugation is assumed. The last column corresponds to the invariant mass spectra of the $p\overline{p}$ system. We draw a number of observations from the calculated probabilities in Table 2. For the first column, the top two rows are marginally consistent with phase space, while the third is consistent, and the last row is inconsistent. The entire second column is consistent with phase space, while in the third column only the third row is consistent, and all others are inconsistent.

Table 2: Probabilities of obtaining the observed result under the null hypothesis that the data is sampled from the phase space model.

$B^0 \to D^{*-} p\overline{p}\pi^+$	$D^{*-}p(\overline{c}duud)$ 1.32×10^{-2}	$D^{*-}\overline{p}(\overline{c}d\overline{uu}\overline{d})$ 0.83	M($p\overline{p}$) 1.22×10^{-4}
$B^0 \to D^{-} p\overline{p}\pi^+$	$D^{-}p(\overline{c}duud)$ 1.78×10^{-2}	$D^{-}\overline{p}(\overline{c}d\overline{uu}\overline{d})$ 1.00	M($p\overline{p}$) 2.58×10^{-4}
$B^0 \to \overline{D}^{*0} p\overline{p}$	$\overline{D}^{*0}p(\overline{c}uuud)$ 0.13	$\overline{D}^{*0}\overline{p}(\overline{c}u\overline{uu}\overline{d})$ 0.68	M($p\overline{p}$) 0.32
$B^0 \to \overline{D}^{0} p\overline{p}$	$\overline{D}^{0}p(\overline{c}uuud)$ 3.51×10^{-4}	$\overline{D}^{0}\overline{p}(\overline{c}u\overline{uu}\overline{d})$ 0.77	M($p\overline{p}$) 3.26×10^{-4}

5 SYSTEMATIC STUDIES

Systematic uncertainties in the ML fit originate from the modeling of the PDFs. We vary the PDF parameters within their respective uncertainties, and derive the associated systematic errors. The SCF fractions can be floated in the fit to data for the decays $B^0 \to D^{*-} p\overline{p}\pi^+$ and $B^0 \to D^{-} p\overline{p}\pi^+$. The differences between MC and data are 8% and 16% for the two decays, respectively. For the systematic uncertainty due to the SCF fraction, we vary the SCF fraction by $\pm10\%$ in the fit according to the above validation from data. We also perform fits to large MC samples with signal and combinatorial background. No bias is observed in these tests.

The systematic errors in the efficiencies are for the track finding (1.2% - 1.4% per track and 2.2% for the slow charged π), particle identification (0.1 - 0.3 %) and π^0 reconstruction (5.6%). The systematic error in each B decay mode arising from variations of the selection criteria is also

Table 3: Summary of the systematic uncertainties for all B modes in this report.

Error source	$D^{*-}p\overline{p}\pi^+$	$D^-p\overline{p}\pi^+$	$\overline{D}^{*0}p\overline{p}$	$\overline{D}^0p\overline{p}$
	(in %)			
Event selection	3.1	3.9	5.6	7.6
Signal model	3.0	3.2	9.0	0.5
Track finding	9.2	8.4	4.8	4.8
π^0 reconstruction	-	-	5.6	-
Particle ID	0.1	0.3	0.1	0.1
Phase space MC	7.5	3.1	-	-
Number of B mesons	1.1	1.1	1.1	1.1
Daughter branching fraction	2.5	6.5	5.3	2.4
Total	13.0	12.2	13.9	9.4

shown in Table 3. The reconstruction efficiencies depend on the final state distributions due to B decay dynamics. As discussed earlier, we assign 7.5% and 3.1% systematic uncertainties to account for the uncertainty on the efficiencies from the phase-space MC simulation for $B^0 \to D^{*-}p\overline{p}\pi^+$ and $B^0 \to D^-p\overline{p}\pi^+$ four-body decays, respectively. Other systematic effects are from event-selection criteria, daughter branching fractions [12], MC statistics, and the number of B mesons in the sample [15]. The contributions to the systematic errors on signal yields are summarized in Table 3.

6 SUMMARY

The B^0 meson decay modes $B^0 \to D^{*-}p\overline{p}\pi^+, D^-p\overline{p}\pi^+, \overline{D}^{*0}p\overline{p}$, and $B^0 \to \overline{D}^0p\overline{p}$ have been studied in a data sample equivalent 113 fb^{-1} of integrated luminosity. Table 4 summarizes the branching fractions obtained for the decays $B^0 \to D^{*-}p\overline{p}\pi^+$, $B^0 \to D^-p\overline{p}\pi^+$, $B^0 \to \overline{D}^{*0}p\overline{p}$ and $B^0 \to \overline{D}^0p\overline{p}$. These results are compared with previous measurements performed by the CLEO [1] and Belle [2] collaborations, when possible, and good agreement is found. The $B^0 \to D^-p\overline{p}\pi^+$ decay has been observed for the first time with the branching fraction $\mathcal{B}(B^0 \to D^-p\overline{p}\pi^+) = (3.80 \pm 0.35 \pm 0.46) \times 10^{-4}$. All results are preliminary.

Table 4: The branching ratios (in units of 10^{-4}) for the B^0 modes are measured here. Statistical (first) and systematic (second) errors are given. The significance includes both the statistical error and the systematic error. Results obtained here are compared with results published by the CLEO [1] and Belle [2] collaborations (when available).

Final state	$\mathcal{B}(10^{-4})$	Significance	Reference $\mathcal{B}(10^{-4})$
$B^0 \to D^{*-}p\overline{p}\pi^+$	$5.61 \pm 0.59 \pm 0.73$	13σ	$6.5^{+1.3}_{-1.2} \pm 1.0$ [1]
$B^0 \to D^-p\overline{p}\pi^+$	$3.80 \pm 0.35 \pm 0.46$	13σ	-
$B^0 \to \overline{D}^{*0}p\overline{p}$	$0.67 \pm 0.21 \pm 0.09$	4.0σ	$1.20^{+0.33}_{-0.29} \pm 0.21$ [2]
$B^0 \to \overline{D}^0p\overline{p}$	$1.24 \pm 0.14 \pm 0.12$	12σ	$1.18 \pm 0.15 \pm 0.16$ [2]

7 ACKNOWLEDGMENTS

We are grateful for the extraordinary contributions of our PEP-II colleagues in achieving the excellent luminosity and machine conditions that have made this work possible. The success of this project also relies critically on the expertise and dedication of the computing organizations that support *BABAR*. The collaborating institutions wish to thank SLAC for its support and the kind hospitality extended to them. This work is supported by the US Department of Energy and National Science Foundation, the Natural Sciences and Engineering Research Council (Canada), Institute of High Energy Physics (China), the Commissariat à l'Energie Atomique and Institut National de Physique Nucléaire et de Physique des Particules (France), the Bundesministerium für Bildung und Forschung and Deutsche Forschungsgemeinschaft (Germany), the Istituto Nazionale di Fisica Nucleare (Italy), the Foundation for Fundamental Research on Matter (The Netherlands), the Research Council of Norway, the Ministry of Science and Technology of the Russian Federation, and the Particle Physics and Astronomy Research Council (United Kingdom). Individuals have received support from CONACyT (Mexico), the A. P. Sloan Foundation, the Research Corporation, and the Alexander von Humboldt Foundation.

References

[1] CLEO Collaboration, S. Anderson *et al.*, Phys. Rev. Lett. **86** (2001) 2732.

[2] Belle Collaboration, K. Abe *et al.*, Phys. Rev. Lett. **89** (2002) 151802.

[3] C-K Chua, W-S Hou and S-Y Tsai Phys. Rev. D **65** (2002) 034003.

[4] W. S. Hou and A. Soni, Phys. Rev. Lett. **86** (2001) 4247.

[5] I. Dunietz, Phys. Rev. D **58** (1998) 094010.

[6] E. Fermi and C. N. Yang, Phys. Rev. **76** (1949) 1739.

[7] J. L. Rosner, Phys. Rev. D **68** (2003) 014004.

[8] R. Jaffe and F. Wilczek, Phys. Rev. Lett. **91** (2003) 232003.

[9] S. Armstrong, B. Mellado and Sau Lan Wu, hep-ph/0312344.

[10] *BABAR* Collaboration, B. Aubert *et al.*, Nucl. Instrum. Methods A **479**, (2002) 1.

[11] S. Agostinelli *et al.*, Nucl. Instrum. Meth. A **506** (2003) 250.

[12] Particle Data Group, S. Eidelman *et al.*, Phys. Rev. D **66**, 010001 (2002).

[13] G. C. Fox and S. Wolfram, Phys. Rev. Lett. **41**, (1978) 1581.

[14] ARGUS Collaboration, H. Albrecht *et al.*, Phys. Lett. B **185** (1987) 218.

[15] *BABAR* Collaboration, B. Aubert *et al.*, Phys. Rev. D **67**, (2003) 032002.

[16] BES Collaboration, J. Z. Bai *et al.*, Phys. Rev. Lett. **91** (2003) 022001.